Available online at www.sciencedirect.com

ScienceDirect

Acta Materialia 80 (2014) 159–171

Acta MATERIALIA

www.elsevier.com/locate/actamat

The microstructure and microtexture of zirconium oxide films studied by transmission electron backscatter diffraction and automated crystal orientation mapping with transmission electron microscopy

A. Garner [a,*], A. Gholinia [a], P. Frankel [a], M. Gass [b], I. MacLaren [c], M. Preuss [a]

[a] Materials Performance Centre, School of Materials, The University of Manchester, Manchester M13 9PL, UK
[b] AMEC, Walton House, Faraday Street, Birchwood Park, Risley, Warrington WA3 6GA, UK
[c] SUPA School of Physics and Astronomy, The University of Glasgow, Kelvin Building, Glasgow G128QQ, UK

Received 24 May 2014; accepted 29 July 2014
Available online 24 August 2014

Abstract

A detailed characterization of nanostructured thin zirconium oxide films formed during aqueous corrosion of a nuclear-grade zirconium alloy (Zircaloy-4) has been carried out by means of two novel, ultra-high-spatial-resolution grain mapping techniques, namely automated crystal orientation mapping in the transmission electron microscope (TEM) and transmission electron backscatter diffraction (t-EBSD). While the former provided excellent spatial resolution with the ability to identify tetragonal ZrO_2 grains as small as ~5 nm, the superior angular resolution and unambiguous indexing with t-EBSD enabled verification of the TEM observations. Both techniques revealed that in a stress-free condition (TEM foil prepared by focused ion beam milling), the oxide consists mainly of well-oriented columnar monoclinic grains with a high fraction of transformation twin boundaries, which indicates that the transformation from tetragonal to monoclinic ZrO_2 is a continuous process, and that a significant fraction of the columnar grains transformed from stress-stabilized tetragonal grains with (0 0 1) planes parallel to the metal–oxide interface. The TEM analysis also revealed a small fraction of size-stabilized, equiaxed tetragonal grains throughout the oxide. Those grains were found to show significant misalignment from the expected (0 0 1) growth direction, which explains the limited growth of those grains. The observations are discussed in the context of providing new insights into corrosion mechanisms of zirconium alloys, which is of particular importance for improving service life of fuel assemblies used in water-cooled reactors.

Keywords: Zirconium oxide; Texture; EBSD; TEM; Corrosion

1. Introduction

The motivation for understanding the microstructure and texture of zirconium oxide films comes from the requirement to improve the aqueous corrosion performance and minimize hydrogen pickup of zirconium alloys, which are used to clad nuclear fuel in light and heavy water reactors. The microstructure of the oxide has been found to directly affect the corrosion performance of zirconium alloys; for example, alloys with low corrosion rates have been observed to exhibit large columnar grains [1]. Their superior corrosion performance is attributed to a reduction in grain boundary area in oxides with large grains, as the grain boundary diffusion coefficient is 10^8 times higher than the bulk diffusion coefficient of the oxide [2]. The grain-to-grain misorientation has also been linked to aqueous

* Corresponding author.
E-mail address: alistair.garner@postgrad.manchester.ac.uk (A. Garner).

http://dx.doi.org/10.1016/j.actamat.2014.07.062
1359-6454/

corrosion performance [3], with more highly textured oxides exhibiting reduced levels of hydrogen pickup and improved corrosion performance. This is attributed to the high fraction of low-angle grain boundaries in highly textured oxide and their associated low mobility for diffusing species. Hydrogen pickup is a major concern for the nuclear industry because it results in hydride formation and embrittlement and can lead to cladding failure via a mechanism known as delayed hydride cracking (DHC) [4]. Despite the correlation between oxide grain orientation and hydrogen pickup, there has been relatively little work attempting to link the microtexture, and thus the grain boundary character distribution in the oxide, to the corrosion performance of zirconium alloys. Previously, zirconium oxide corrosion films have provided a significant challenge for grain orientation mapping due to their fine grain size (some grains are less than 30 nm), high levels of residual stress, complex microstructural morphology and dual phase nature, a mixture of metastable tetragonal and stable monoclinic zirconia [1].

The technique of electron backscatter diffraction (EBSD) has made considerable advances in recent years; with improvements in both hardware and software it has now become possible to detect, and accurately index, Kikuchi patterns from ultra-fine-grained materials such as zirconium oxide. The best possible resolution is achieved on electron-transparent samples in transmission geometry, using a technique termed transmission EBSD (t-EBSD) [5,6]. Automated crystal orientation mapping in the transmission electron microscope (TEM) can also be used to map the phase and orientation of such fine-grained microstructures [7]. The electron beam is scanned across the sample and transmission electron diffraction spot patterns are recorded and matched to calculated templates in order to deduce phase and orientation information. This TEM technique offers improved lateral spatial resolution over t-EBSD; however, angular and phase detection accuracy are reduced due to the low sensitivity and ambiguity of electron diffraction spot patterns. Overlapping grains can also cause problems when using transmission techniques on such a fine-grained microstructure as zirconium oxide. The overlapping of grains in the TEM will result in the formation of composite diffraction patterns, which can lead to problems during the template matching process. However, in t-EBSD, the Kikuchi patterns have been shown to originate primarily from the exiting surface of the sample [6], therefore the occurrence of composite patterns from overlapping grains is reduced. In the present study the strengths of both transmission-based orientation-mapping techniques were combined to investigate the microstructure, microtexture and grain boundary distribution of oxide films formed on a zirconium alloy as a consequence of extended corrosion in superheated pressurized water.

Previous attempts to measure the orientation of the grains that make up the oxide formed on Zircaloy-4 have been carried out using X-ray diffraction (XRD) [8–11] texture measurements. These investigations have demonstrated that a strong fibre texture forms in the monoclinic oxide on Zircaloy-4 during aqueous corrosion, with the $(10\bar{3})$ [11], $(10\bar{4})$ [8] or $(10\bar{5})$ [10] planes parallel to the sample surface. The discrepancy between these studies is due to the fact that the monoclinic grains can adopt a range of orientations. Theoretical calculations have shown that monoclinic grains with orientations ranging between $(10\bar{3})$ and $(10\bar{6})$ reduce the in-plane surface area and so minimize the transformation stress associated with the metal-to-oxide transformation during oxide growth [12]. The orientation of the tetragonal phase has also been measured using XRD [11]; a (001) texture was found to form on Zircaloy-4, which is again the orientation with the smallest in-plane surface area for this phase. It is important to note that texture measurement via XRD is a bulk technique sampling a comparatively large volume and the non-destructive nature of these measurements allows the stress state in the oxide to be maintained. However, it does not allow for direct characterization of grain-to-grain misorientations. TEM observations have shown qualitatively a similar texture in the monoclinic phase formed on Zircaloy-4, and also revealed a more well-defined texture away from the metal–oxide interface [1]. These observations were made using a large diffraction aperture, which samples the average texture over a relatively large area of hundreds of nm, and as such are not correlated with the oxide microstructure. High resolution TEM (HRTEM) has been utilised to directly measure the orientations of individual oxide grains [13–16]. The observations reveal that the oxide consists of a large proportion of well-oriented columnar monoclinic grains, and a small number of more randomly oriented equiaxed monoclinic and tetragonal grains. It is important to note that XRD analysis of the oxide generally reports significantly higher volume fractions of tetragonal phase than TEM analysis on foils where the stresses have been relieved [13,16]. The oxide has also been observed to contain a high fraction of twin boundaries [15], which are thought to form as a result of the tetragonal-to-monoclinic transformation during oxide growth. However, due to the time-consuming nature of manual TEM orientation analysis, these TEM investigations tend to concentrate on a small number of grains and thus lack statistical significance, which is of concern considering the heterogeneity of the oxide microstructure [16].

Zircaloy-4 exhibits cyclic corrosion kinetics during aqueous corrosion in an autoclave environment, as shown in Fig. 1. At a critical oxide thickness, the oxide loses its protectiveness and accelerated corrosion kinetics are observed; this region in the corrosion curve is often termed the transition. After the transition, the oxide regains its protectiveness and the process repeats itself in a cyclic manner until a period of approximately linear growth develops, known as breakaway corrosion. During oxide growth, the transformation from zirconium to zirconium oxide causes high levels of compressive stress in the oxide, which has been shown to decrease with distance from the interface [9,17]. Stress relaxation in the oxide is postulated to be

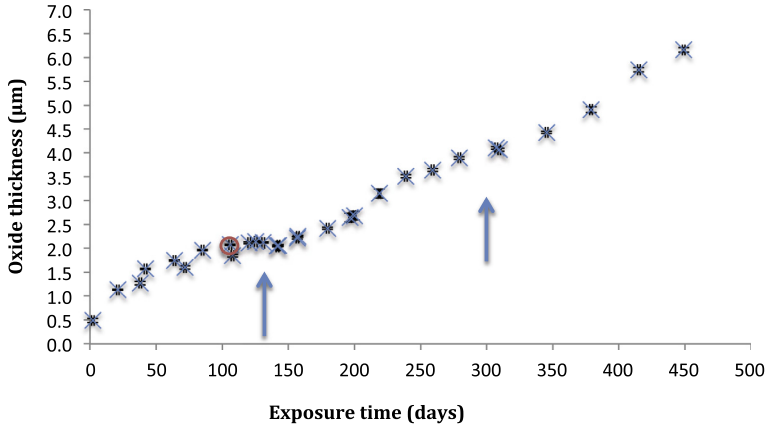

Fig. 1. Corrosion curve for Zircaloy-4 exposed to simulated PWR conditions at 350 °C. The circle represents the exposure time of the sample analysed in this work. Arrows represent approximate exposure times where transition in corrosion kinetics are observed.

caused by a combination of creep in the metal substrate [18], lattice expansion from hydrogen pickup [19] and also crack formation in the oxide [17]. This reduction in stresses could cause the transformation of the stress-stabilized tetragonal grains and lead to the transition in corrosion kinetics; this theory is supported by a reported increase in the stress levels in the monoclinic phase prior to transition [20]. The tetragonal-to-monoclinic phase transformation has an associated volume increase (3–7%) [21–25] and large shear strain (14–18%) [23–25] and has often been postulated to drive the formation of cracks and linking up of porosity in the oxide, which subsequently provide fast tracks for diffusing species [17,26,27]. However, there is no clear evidence to date as to whether the majority of oxide grains start out as tetragonal or monoclinic, and the extent and cause of transformation throughout the oxide is unknown. Previous studies have been unable to characterise the oxide grain boundary network throughout the oxide, and as such the development of grain boundaries and the effect on corrosion behaviour are also unknown. The present work seeks to answer some of these questions using ultra-high-resolution grain mapping techniques. The orientation, phase and grain boundary information are used to provide insight into the nature and extent of the transformation and how this affects the corrosion behaviour of zirconium alloys.

2. Experimental methods

2.1. Sample preparation

A cross-sectional sample was prepared for microtexture examination by focused ion beam (FIB) milling [28] using the in situ lift-out technique on a FEI Nova Nanolab DualBeam instrument at the University of Glasgow. This technique allows for the targeted preparation of relatively large electron transparent areas of fairly uniform thickness, and is particularly useful for cross-sectional oxide films where there is a composite of ceramic and metallic material. The sample was prepared with the surface parallel to the original rolling direction from a corrosion coupon of sheet Zircaloy-4 that had been exposed to simulated pressurized water reactor (PWR) conditions for 106 days at 350 °C. The composition of the alloy is shown in Table 1 and the oxide thickness generated after this time was calculated from the weight gain measured to be ~2.1 µm (1 µm of oxide is equivalent to a weight gain of 15 mg dm^{-2} [29]). The corrosion curve for this alloy (Fig. 1) demonstrates that this oxide thickness represents an exposure time just prior to transition.

2.2. Transmission EBSD

All EBSD measurements were performed on an FEI Magellan 400 XHR scanning electron microscope (SEM) at the University of Manchester equipped with a Nordlys-Nano EBSD detector. The spatial resolution of EBSD is dependent on the interaction volume of the electron beam in the sample. The best possible resolution is achieved using a field emission gun, which allows for a high current density and a small spot size. In order to further improve the resolution, the interaction volume of the sample needs to be minimized. This was achieved in the present case by mounting the FIB sample in the SEM with the EBSD detector positioned beneath the sample in transmission geometry, as shown in Fig. 2. An accelerating voltage of 30 keV was used with a probe current of 1.6 nA and a step size of 10 nm. The working distance was set at 2 mm and the sample was tilted 20° away from the detector. A small tilt angle was used as a reduction in tilt angle has previously been shown to give improved spatial resolution [6]. The Kikuchi patterns taken at 8×8 binning were indexed at 60 Hz using the AZtec software suite with the crystallographic information for phases zirconia and zirconium given in Table 2. The orientation analysis of both t-EBSD and TEM data was performed using the Channel 5 software suite developed by Oxford Instruments HKL.

Table 1
The chemical composition of Zircaloy-4, alloying additions only listed, balance is zirconium.

Sn (wt.%)	Fe (wt.%)	Cr (wt.%)	O (wt.ppm)	C (wt.ppm)	Si (wt.ppm)
1.45	0.21	0.10	970	45	46

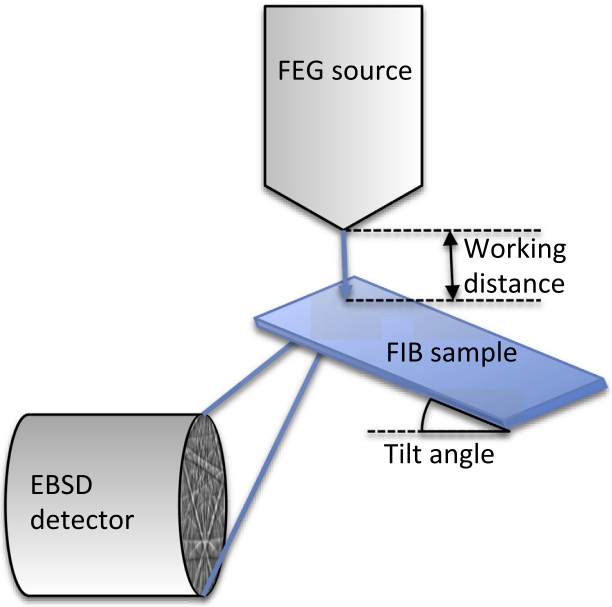

Fig. 2. Schematic diagram of experimental set up for t-EBSD.

2.3. Automated crystal orientation mapping with TEM

All TEM experiments were performed on an FEI Tecnai F30 FEG-TEM at the University of Manchester, operating at 300 keV with a camera length of 7.1 cm. The spot pattern collection and analysis were carried out using the ASTAR automated crystal orientation mapping system [30]. A precession angle of 0.8° was used in order to increase the number of diffraction spots and reduce dynamical effects, which has been shown to improve the quality of phase/orientation maps using this system [31]. Firstly, the beam was scanned across the sample and electron diffraction patterns saved at each position; a step size of 5 nm was used in this investigation with an acquisition rate of 50 fps. Theoretically generated templates were produced for each phase present in the sample; the crystallographic information for each phase was extracted from crystal information files (CIFs) produced from powder diffraction data, as detailed in Table 2. The acquired patterns were then automatically matched with the banks of generated templates using the template matching method [30]. The degree of matching between the experimental and calculated patterns is given by the correlation index and can be used to reveal grain boundaries and other microstructural features in a similar way to band contrast in EBSD. For each solution, an orientation reliability index is also given, which was calculated using the ratio of the two highest values of the correlation index. If there are two different solutions with similar correlation index values, this will produce a low reliability value. In general, solutions with a reliability >15 can be assumed to be correct [30]. Phase reliability was also calculated for each solution from the ratio of the two highest values of the correlation index for each phase. The software automatically assigns the solution to the orientation and phase with the highest correlation index.

3. Experimental results

3.1. t-EBSD

The area of t-EBSD analysis in relation to the FIB sample is indicated in Fig. 3. A band contrast image taken from region A of the Zircaloy-4 FIB sample is shown in Fig. 4a. Equiaxed grains are clearly shown on the outer surface of the oxide, with larger columnar grains forming towards the metal–oxide interface. The columnar grains are oriented perpendicular to the interface. This type of grain

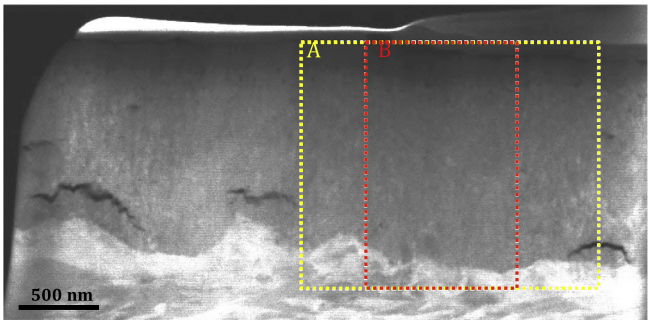

Fig. 3. Secondary electron image of cross-sectional Zircaloy-4 FIB sample showing approximate areas of analysis. Yellow box indicates area for t-EBSD analysis (region A) and red box indicates TEM analysis area (region B). (For interpretation of the references to color in this figure legend, the reader is referred to the web version of this article.)

Table 2
Crystal structures used for t-EBSD and TEM analysis.

Crystal structure	a (Å)	b (Å)	c (Å)	α (°)	β (°)	γ (°)	ICSD ID	Ref.
Hexagonal Zr	3.23	3.23	5.14	90	90	120	53785	[32]
Monoclinic ZrO_2	5.17	5.23	5.34	90	99.25	90	26488	[33]
Tetragonal ZrO_2	3.59	3.59	5.18	90	90	90	66781	[34]

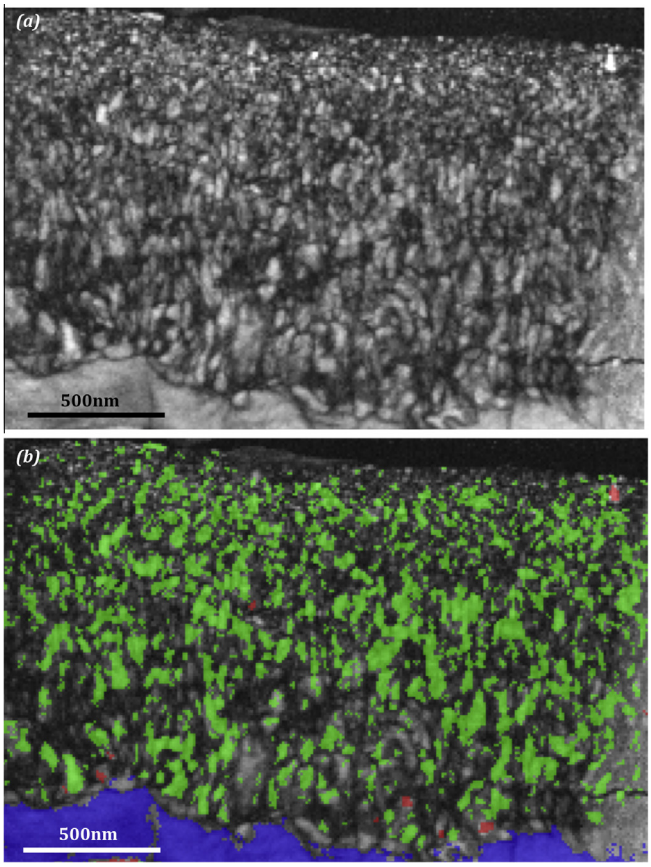

Fig. 4. t-EBSD maps of region A of cross-sectional Zircaloy-4 FIB sample: (a) band contrast map, (b) phase map (monoclinic ZrO_2 is shown in green, tetragonal ZrO_2 is shown in red and zirconium metal is shown in blue). (For interpretation of the references to color in this figure legend, the reader is referred to the web version of this article.)

morphology is commonly reported in TEM investigations [1,13,14]. The equiaxed grains are generally 10–50 nm in diameter and the columnar grains have a length between 100 and 200 nm. This is in agreement with grain size measurements using line broadening in XRD [29] and directly in TEM [1]. The phase map of the same region is shown in Fig. 4b. The major oxide phase is monoclinic, although some small tetragonal grains are also visible. The volume fraction of the tetragonal phase as calculated from the image is ~1%, which is significantly below the phase fraction range of 4–15% measured by conventional and synchrotron XRD [9,35]. This difference may be explained by the stress relaxation that occurs during TEM sample preparation, which will lead to transformation of larger stress-stabilized tetragonal grains. Additionally, as only size-stabilized tetragonal grains will remain in a TEM foil, some tetragonal grains may also be smaller than the resolution limit of transmission EBSD (~10 nm).

The orientation map of region A for the monoclinic phase is shown in Fig. 5a. Macrotexture measurements via XRD have shown that the main texture component in monoclinic oxide is between the $(10\bar{3})$ and $(10\bar{5})$ fibre [8–11]. For t-EBSD in the sampled region, the $(10\bar{3})$ texture component was the most common, and the colouring in Fig. 5 is therefore based on degrees away from this component. It can be seen from the frequency plot that the majority of the oxide grains are within ~10° of this texture component, and are represented by the blue family of grains. However, Fig. 5 also highlights that a noticeable number of grains are oriented away from this fibre. The equiaxed grains on the outer surface of the oxide appear to have a larger deviation from the main fibre component than the columnar grains that make up the bulk of the oxide. Towards the metal–oxide interface, a significant fraction of grains are also visible with orientations away from the main fibre component. XRD experiments have identified a second fibre component in monoclinic zirconia [10], which is postulated to correspond to the light green family of grains in Fig. 5, oriented ~50° away from the main texture component. The orientation data can also be represented on pole figures, as shown in Fig. 6. The pole figures show that the monoclinic grains generally have rotational freedom about the oxide growth direction. The $(11\bar{1})$ planes are restricted to polar angles in the range ~30–50°, the (1 1 1) planes are oriented > 60°, the (0 0 2) planes are oriented within ~20° of the oxide surface and the $(10\bar{3})$ planes are oriented within 10° of the sample surface, in agreement with XRD measurements on Zircaloy-4 [8,10,11]. Fig. 6 also shows a small number of orientations away from the main fibre component; the light green regions ~50° from the main fibre are again seen here.

The indexing rate of the t-EBSD technique in this investigation is ~40% and as such the number of complete grain boundaries identified is low. However, due to the precision of orientation analysis using EBSD patterns (generally <1° for absolute misorientations [36]), the grain boundary regions that are visible are still thought to provide some useful insight into the nature of grain boundaries formed in zirconium oxide. The monoclinic misorientation distribution is shown in Fig. 7. It demonstrates that the most frequently indexed grain boundaries in the oxide are described by 90° and 180° misorientations. These are generally associated with the tetragonal-to-monoclinic transformation and form as a result of twin-related variant formation in zirconium oxide [37], which will be discussed in more detail later.

3.2. Automated crystal orientation mapping with TEM

The combined phase reliability and orientation map of monoclinic oxide in region B (see Fig. 3) is shown in Fig. 8a, which displays the expected oxide nanostructure comparable to the t-EBSD observations. The map reveals a fine level of detail with grains as small as ~5 nm in the outer region of the oxide. The colouring is based upon degrees away from the ~$(10\bar{3})$ fiber component, as described previously. The frequency plot (Fig. 8b) indicates that the majority of monoclinic grains are oriented within 10° of this fibre, in agreement with the previous t-EBSD observations. Again, as with the t-EBSD orientation map, the equiaxed grains near the outer surface of the

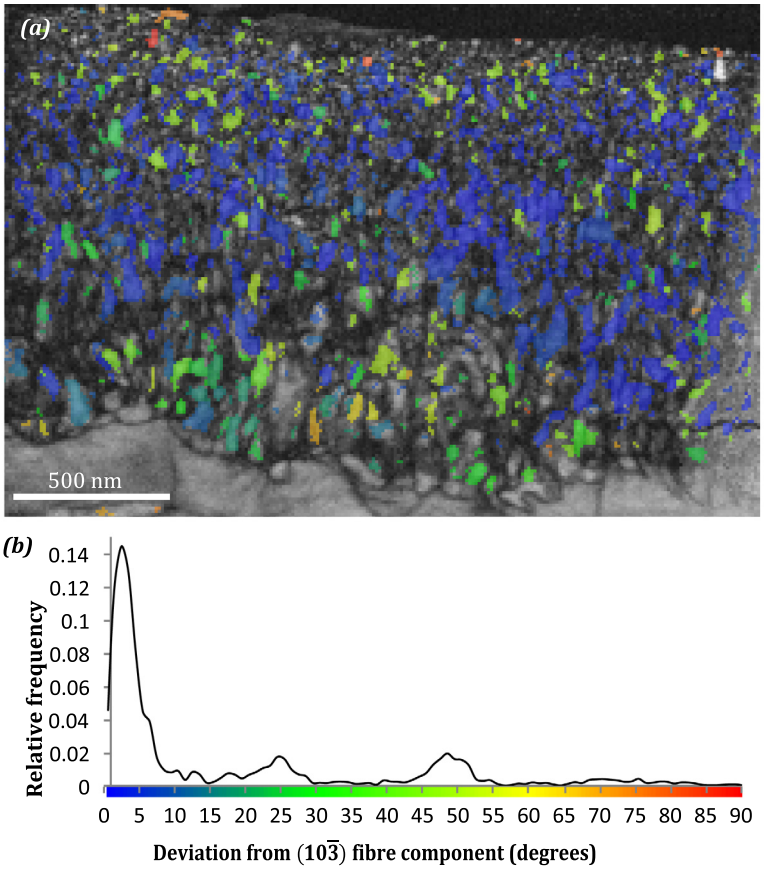

Fig. 5. (a) Orientation map of region A of cross sectional Zircaloy-4 FIB sample from t-EBSD analysis. (b) Legend shows colouring as degrees away from main (1 0 3) fibre component as well as the relative frequency of deviation. (For interpretation of the references to colour in this figure legend, the reader is referred to the web version of this article.)

oxide appear to have a greater misorientation from the main fibre component than the columnar grains visible in the middle of the oxide. Also, in agreement with the t-EBSD observations, there is a significant number of large monoclinic grains that appear to be oriented away from the main fibre component towards the metal–oxide interface. The corresponding (1 0 $\bar{3}$) monoclinic pole figure is shown in Fig. 10a, which further confirms that the distribution of poles agrees with the t-EBSD data. Even less obvious features, like the grains orientated ~50° away from the (1 0 $\bar{3}$) texture component, are again seen here.

The combined phase reliability and orientation map of tetragonal oxide in region B is shown in Fig. 9a. Due to the improved resolution of the TEM technique, small tetragonal grains are also now visible throughout the oxide. The tetragonal grains range in diameter from ~5 to 30 nm and are mostly equiaxed; however, at the metal–oxide interface some larger tetragonal grains are visible. Towards the outer surface of the oxide there is a layer of small tetragonal grains that coincides with the equiaxed grain region reported here and in the literature [1]. There is also a region of small (5–20 nm) tetragonal grains located ~1 μm from the metal–oxide interface. The tetragonal phase fraction of region B is ~3%, which is significantly higher than the measured tetragonal phase fraction from region A by t-EBSD measurements due to the improved resolution of this technique. The critical grain size for stabilization of the tetragonal phase has been previously estimated to be ~30 nm [38]. In the present study, the majority of tetragonal grains are below this critical size; however, it is postulated that the large tetragonal grains close to the interface could be stabilized by compressive stresses that may remain in the region of the undulating interface. Following the argument of smallest in-plane surface area to minimize transformation stresses [10,12], the tetragonal grains that are favourably oriented for growth should have their (0 0 1) planes parallel with the metal–oxide interface. This has been verified previously by non-destructive oxide texture analysis on Zircaloy-4 using XRD [11]. The tetragonal orientation map is therefore colour-coded according to degrees away from the (0 0 1) fibre. In contrast to expectations, the orientation map indicates that the there is a large spread in the orientation of the tetragonal grains and that a significant fraction are oriented away from this fibre component, which can also be seen from the (0 0 1) pole figure presented in Fig. 10b. As this contradicts pole figures measured by XRD when the oxide was fully exposed to the stress field [11], it seems likely that the tetragonal grains measured in this investigation represent those grains that were not favourably oriented for

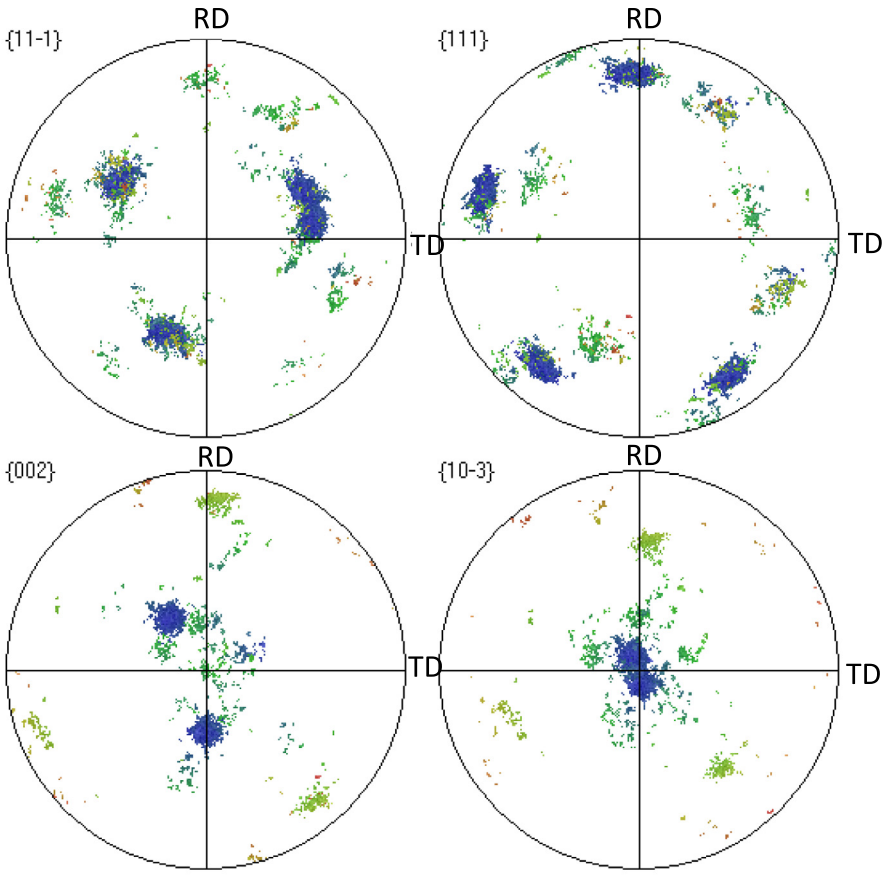

Fig. 6. Pole figures for the 111, 111, 002 and 103 planes of monoclinic oxide formed on cross-sectional Zircaloy-4 FIB sample as measured by t-EBSD. Colours represent degrees away from main texture component as shown in legend in Fig. 5. (For interpretation of the references to colour in this figure legend, the reader is referred to the web version of this article.)

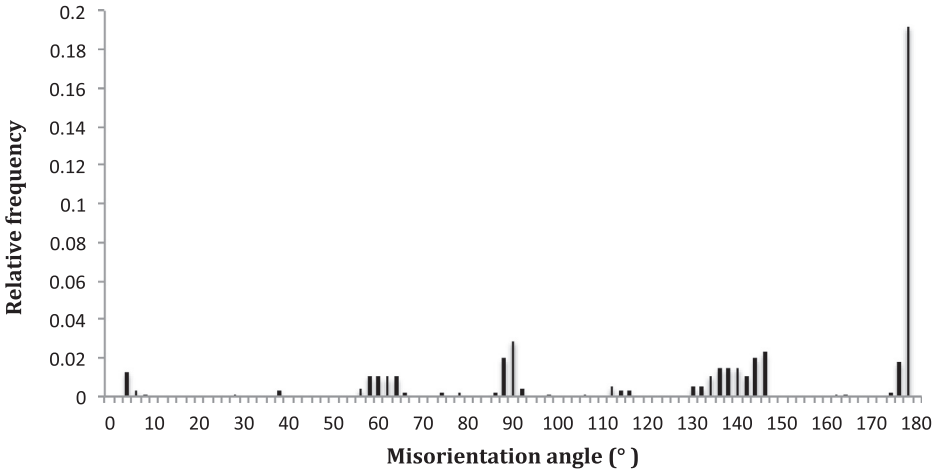

Fig. 7. Correlated misorientation angle distribution of monoclinic oxide formed on Zircaloy-4 as measured by t-EBSD.

growth and so remain at a small enough size to be stable, even when most of the compressive stress in the oxide is relieved. In contrast to this, the tetragonal grains that are favourably oriented are more likely to grow above the critical size for stabilization and so are only stable in the presence of stress in the oxide. It is noted here that the orientation reliability for the monoclinic phase is significantly higher than for the tetragonal phase. This is due to the smaller grain size of the tetragonal phase. Consequently there are likely to be increased numbers of overlapping grains over the thickness of the FIB foil, resulting in the formation of composite diffraction patterns. However, the orientations of both phases have been verified using t-EBSD, which is not as sensitive to overlapping grains.

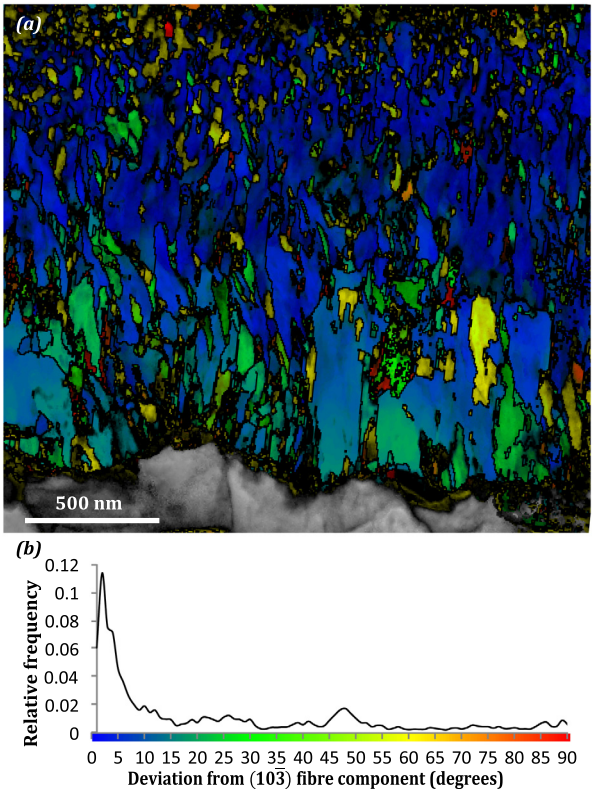

Fig. 8. (a) Combined monoclinic orientation and phase reliability map from automated crystal orientation mapping in TEM, taken from region B of cross-sectional Zircaloy-4. (b) Legend shows colouring as degrees away from main fibre component as well as the relative frequency of deviation. (For interpretation of the references to colour in this figure legend, the reader is referred to the web version of this article.)

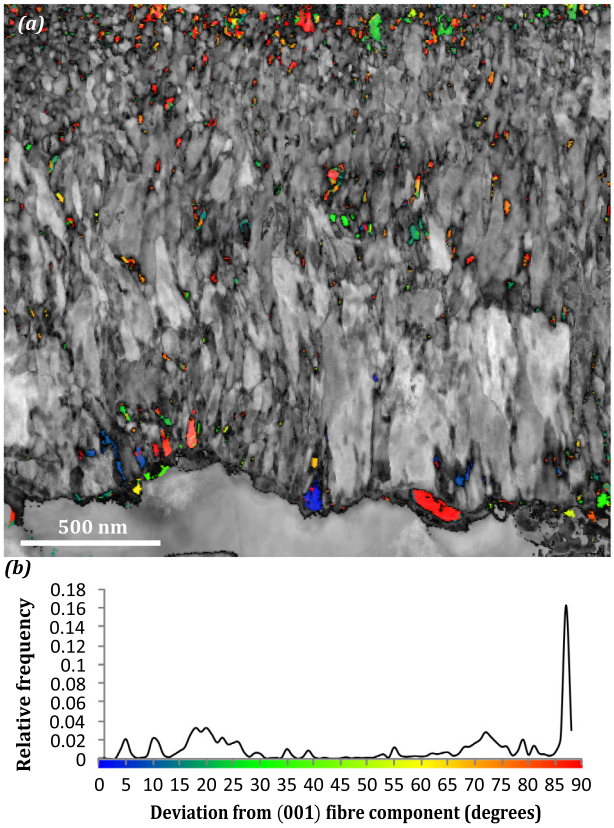

Fig. 9. (a) Combined tetragonal orientation and phase reliability maps from automated crystal orientation mapping in TEM, taken from region B of cross-sectional Zircaloy-4 FIB sample. (b) Legend shows colouring as degrees away from main fibre component as well as the relative frequency of deviation. (For interpretation of the references to colour in this figure legend, the reader is referred to the web version of this article.)

The majority of tetragonal grains identified using t-EBSD have the *c*-axis aligned away from the oxide growth direction, in agreement with the TEM observations.

Due to the high indexing rate of the TEM technique, entire grain boundary maps of region B can be calculated and are shown in Fig. 11. Fig. 11 highlights the positions of the 90°, 180° and 142° boundaries. It can be seen that a large proportion of the grain boundaries are made up of these types of boundaries and together make up ~60% of the total grain boundary area of region B. According to the literature, two main types of twin boundary are expected in monoclinic zirconia, identified as 90.8° and 180° rotations about the [0 0 1] crystallographic direction of the monoclinic unit cell [15,39]. These types of boundary are the most common of the identified angle/axis misorientations and together make up ~14% of the total boundary length in region B. Misorientations identified by 180° rotations around the [1 0 $\bar{1}$], [1 0 0] and [1 0 1] directions have also been identified and together make up ~12% of the total boundary length of region B. Twin boundaries have a highly ordered atomic structure [40] and therefore are predicted to have a low mobility for diffusing species. There is also a high fraction of boundaries defined by a ~142° rotation around the [$\bar{1}$ 0 3] direction, accounting for ~9% of the total boundary length, which are highlighted in Fig. 11c. According to Gertsman [37], there is a possible twin-type interface defined by a misorientation of 143.1° about [$\bar{3}$, 0, 1, 17] (this axis makes a small angle of 7.5° with [$\bar{1}$ 0 3]). This is described by Gertsman et al. [37] as a Σ30 CSL, according to the approximations used in that work. This same orientation relationship can also be expressed as a twin misorientation of 180° about [3 1 1]. The latter relationship probably describes these boundaries better as the boundary normals for such boundaries in Fig. 11c are mainly perpendicular to the strong (1 0 $\bar{3}$) fibre texture direction close to the surface normal. Thus, these boundaries must have a habit plane at an angle close to 90° to the normal to (1 0 $\bar{3}$) – this is true of [3 1 1] but not [$\bar{3}$, 0, 17] (which is almost parallel to (1 0 $\bar{3}$)). This all suggests that these particular boundaries are a frequently occurring twin resulting from the tetragonal-to-monoclinic phase transformation, but further work would be required to unambiguously determine the habit plane and consequently to understand the precise formation mechanisms and reasons for stability of these boundaries.

There are also regions where there appears to be a number of tightly packed grain boundaries inside a single oxide grain. These are not believed to be real grain boundaries and are attributed to the 180° ambiguity problem when

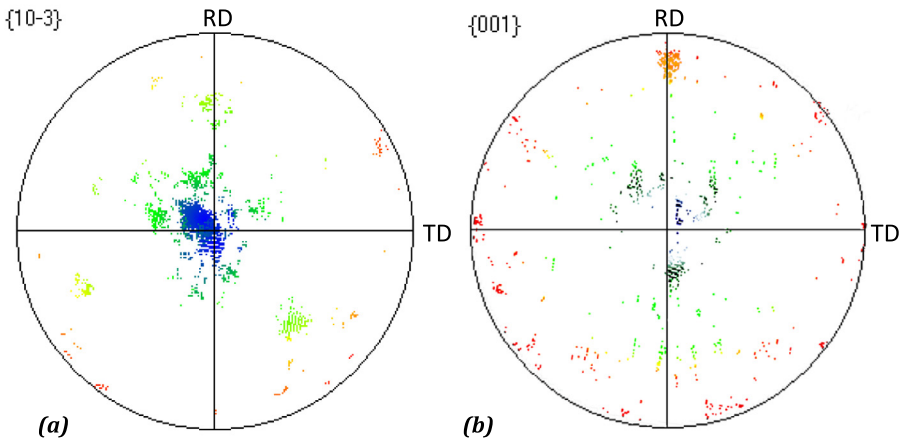

Fig. 10. Pole figures for region B of the Zircaloy-4 FIB sample as measured by automated crystal orientation mapping in TEM: (a) $(10\bar{3})$ monoclinic pole figure, (b) (001) tetragonal pole figure. Colouring based on degrees away from respective fibre components as shown in Figs. 8 and 9. (For interpretation of the references to colour in this figure legend, the reader is referred to the web version of this article.)

indexing electron diffraction spot patterns [7]. The use of precession should reduce this error but it can be seen from the map that this type of misindexing still creates an increased uncertainty for the absolute fraction of 180° twin boundaries identified by this technique. However, it is noted that the misorientation angle distribution measured by t-EBSD, which has unambiguous indexing due to its large solid angle, also shows a high fraction of 180° misorientations (Fig. 7).

4. Discussion

4.1. Twin formation

Numerous diffraction studies have established that the tetragonal phase fraction decreases from the metal–oxide interface towards the outer surface of the oxide, confirming continuous tetragonal-to-monoclinic phase transformation as the metal–oxide interface proceeds inwards [8,17,20,38,41]. Stabilization of the tetragonal phase at ambient and reactor operating temperatures is widely considered to be due to a combination of stress [20], grain size [42] and dopant effects [41]. Therefore, as the oxide grows into the metal, one or more of these constraints are partly relaxed, which results in a martensitic transformation from tetragonal to monoclinic zirconium oxide. Bulk techniques have so far failed to differentiate between these different stabilization mechanisms as the information cannot be correlated directly with the oxide microstructure. Twin formation in zirconia has been studied extensively due to its importance in transformation toughening of structural ceramics [37,43,44]. The formation of twin boundaries in zirconium oxide is postulated to be governed by a process known as twin variant selection whereby the formation of a twin-related variant opposes the shape strain in the adjacent variant and thus reduces the overall shear strain of the region [37]. The large fraction of transformation twin boundaries observed in the oxide suggests that the majority of the monoclinic grains were transformed from the tetragonal phase. It has previously been suggested that the interaction of two twin boundaries can lead to the formation of a third [39]. It is therefore theoretically possible that the entire oxide grain boundary network can be composed of twin boundaries. The frequency and distribution of the twin boundaries identified in this study indicate that the transformation from tetragonal to monoclinic zirconia is a continuous process.

4.2. Orientation relationships

There have been many attempts over the years to derive an orientation relationship between zirconium metal and zirconium oxide. Early TEM observations by Ploc [45] on single Zr crystals concluded that there is no unique orientation relationship between α-Zr and monoclinic oxide. More recently, HRTEM observations on the interface of oxidised Zircaloy-4 have suggested the following orientation relationship [13]:

$$(10\bar{1}0)_{Zr}//(111)_{m}$$

Other authors have found the following relationship using HRTEM on the interface of oxidised ZIRLO® [16]:

$$(10\bar{1}0)_{Zr}//(200)_{m} \quad \text{or} \quad (020)_{m}$$

These relationships were derived from observations on small numbers of oxide grains and in many cases were not unique, even in the small area typically analysed by HRTEM. One of the reasons for this confusion could be that a large fraction of the oxide grains started out as the metastable tetragonal phase. The high fraction of transformation twin boundaries identified in this study seems to suggest that this is in fact the case. Therefore, there are most likely two main sets of orientation relationships: one between zirconium and tetragonal ZrO_2 and the other

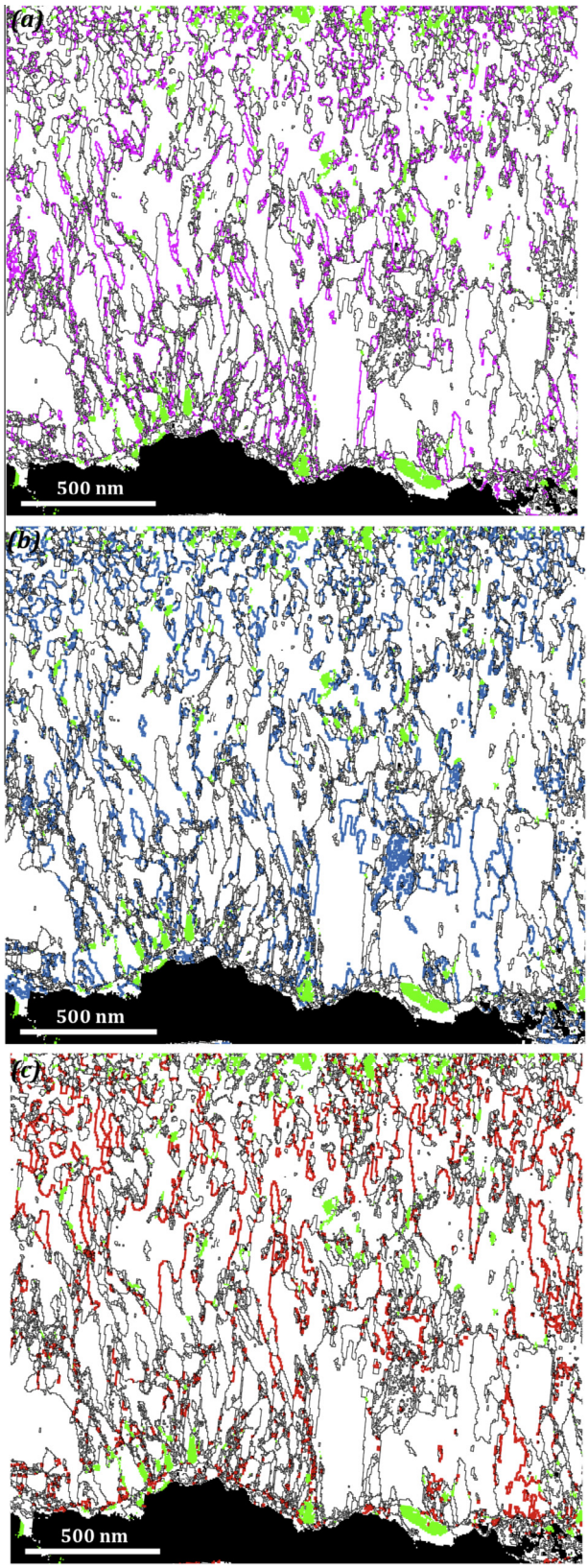

Fig. 11. Grain boundary maps for region B of cross-sectional Zircaloy-4 FIB sample: (a) 90°, (b) 180° and (c) 142° boundaries highlighted in purple, blue and red, respectively. Misorientations >10° shown in black if not highlighted and tetragonal grains are shown as green. (For interpretation of the references to color in this figure legend, the reader is referred to the web version of this article.)

between tetragonal and monoclinic ZrO_2. More recently, synchrotron XRD observations have demonstrated that in protective oxides, an interfacial tetragonal phase forms according to the following orientation relationship with the substrate [46]:

$$(10\bar{1}0)_{Zr}//(002)_t$$

However, this relationship was derived from model alloys with the $(10\bar{1}0)$ planes of the metal substrate aligned with the surface of the sample, whereas conventionally processed Zircaloy-4 exhibits a split basal texture [47]. In the single zirconium grain present in the FIB sample investigated here, the (0002) basal pole is aligned in the normal–transverse direction plane of the sample, in agreement with the expected texture. Upon examination of the tetragonal (001) pole figure in Fig. 10b, it appears that there is no specific orientation relationship between the substrate and tetragonal oxide. This could be due to the fact that the $(10\bar{1}0)$ plane is not parallel to the surface in Zircaloy-4 and therefore lattice matching cannot occur during the first stages of oxide growth [12]. Therefore, many different orientations can form on a single zirconium grain, explaining the distribution of orientations shown in Fig. 10b. Out of these orientations, those with the (001) planes most parallel to the interface will be favourably oriented for growth as they have the smallest in-plane surface area. The rotation of these orientations around the growth direction axis will not affect the in-plane surface area, and so there is no preferential selection of directions and a fibre texture is formed.

The results presented here suggest that the tetragonal phase forms first in order to allow for the development of favourably oriented monoclinic grains. It is therefore likely that an orientation relationship exists between the tetragonal and monoclinic phases. Out of all the possible orientation relationships between monoclinic and tetragonal zirconium oxide, one of the most energetically favourable in order to reduce the lattice strain is given by [48]:

$$(100)_t||(100)_m$$

This orientation relationship was also observed experimentally on thin zirconia films during in situ heating in a TEM [25]. If the well-aligned tetragonal grains transform to the monoclinic phase according to this relationship, then due to the ~99° β angle in the monoclinic unit cell, monoclinic planes with the smallest surface area will be oriented parallel to the interface. It is therefore difficult to ascertain whether the stress is driving the formation of the tetragonal or the monoclinic phase, as both would result in the observed monoclinic texture. The results presented here, however, suggest that the stress caused by oxide formation drives the formation of the tetragonal texture, which then transforms to give the observed monoclinic texture.

Theoretically, the $(10\bar{6})$ orientation has the smallest surface area of all the possible monoclinic orientations [12] and should also be the major orientation during transformation of the well-aligned tetragonal grains (with the

(0 0 1) parallel to sample surface). Planes with slightly larger surface areas are more commonly measured during bulk texture measurement [8,10,11] and in the present work. The reasons for this are currently unclear; however, Lin et al. [12] suggest that the discrepancy could be due to the anisotropic stiffness of the different orientations, which could mean that certain oxide orientations are more energetically favourable, even though they have slightly larger surface areas.

4.3. Relation to corrosion process

In the early stages of corrosion, the oxide is characterised by small, mainly tetragonal equiaxed grains with a large range of orientations. The layer is thin, non-protective and contains high levels of porosity [49]. Consequently, the corrosion rate is fast in the early stages of corrosion, as can be seen in Fig. 1. As the oxide thickens, the corrosion rate begins to slow, allowing time for the growth of suitably oriented tetragonal grains. As larger, well-oriented grains begin to grow, the grain boundary area and the misorientation between grains are reduced. This restricts the fast paths for diffusing species and so the corrosion rate slows down further, as can be seen after an exposure time of ~30 days in Fig. 1. The grain boundary maps in Fig. 11 show twin boundaries surrounding large monoclinic grains, confirming that some tetragonal grains are allowed to grow and remain tetragonal, stabilized by stress [2,20] and possibly assisted by dopants in the oxide [41]. When the stress in a particular region of oxide decreases to a critical point away from the interface, the well-oriented tetragonal grains in that region will transform to monoclinic grains of similar orientation. The majority of the oxide at this point is therefore composed of highly oriented protective columnar grains. This microstructure is thus resistant to diffusing species and could contribute to the "plateau" region prior to the transition on Fig. 1. The results presented here show that the transformation causes the formation of twin boundaries between columnar monoclinic grains, many of which are almost completely coherent and thus have low interfacial energies [50]. The development of these boundaries is therefore not assumed to have a detrimental effect on the corrosion behaviour. It can be seen from the microstructures presented in this investigation that the columnar grains do not grow indefinitely. Once they reach a certain length, they appear to stop growing and new grains form. Motta et al. [35] suggest that the reason for the termination of columnar grain growth is stress accumulation due to small mismatches between the grain growth direction and the ideal orientation. From the data presented here, it is difficult to say whether this is the case. However, it has been shown that there is a considerable spread of orientations in the oxide and therefore the majority of grains are not perfectly oriented and will not be able to grow beyond a critical size. New tetragonal grains will then begin to form with a variety of orientations where the columnar grains terminate, resulting in the cluster of small tetragonal grains visible ~1 μm from the interface in Fig. 9a.

As previously mentioned, the sample used in this investigation is positioned just before the first transition on the corrosion curve (Fig. 1). A sudden increase of stresses in the monoclinic phase has been reported to occur just before transition [17], which suggests that there is a significant transformation from the tetragonal phase at this point. The associated volume increase and shear strain, as shown schematically in Fig. 12, would lead to the formation of cracks and pores, which would provide a fast track for diffusing species. Examination of the microstructure and grain boundary network presented in this investigation suggests that the transformation is a continuous process. It appears therefore that a significant amount of transformation can occur in the oxide whilst still remaining protective. It is therefore postulated that in the early stages of corrosion, the local nature of the transformation and distance from the interface allow for any associated porosity to remain isolated and not interconnected in the growth direction. As oxide growth continues, it appears that there is a point where the stress in the protective oxide layer close to the interface drops below a critical value, leading to increased levels of transformation and the onset of interconnected porosity. It has previously been reported that undulations in the metal–oxide interface can lead to lateral cracking of the oxide close to the interface in pre-transition oxides [51]. These lateral cracks will not provide fast tracks for diffusing species provided they do not become interconnected in the growth direction but could contribute to increased stress relaxation in the oxide leading up to the transition. As the oxide growth front slows down, the continued stress relaxation mechanisms in the oxide result in a

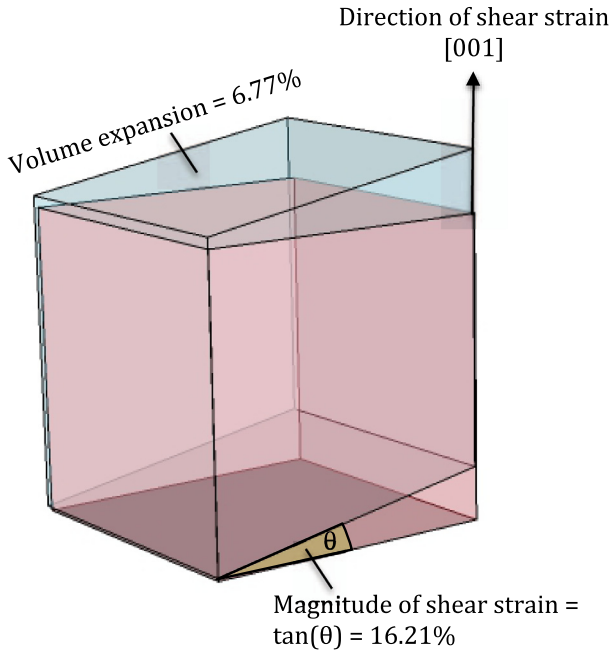

Fig. 12. Schematic of the tetragonal-to-monoclinic transformation.

region of reduced stress that increasingly approaches the metal–oxide interface. At a critical point, this reduction in stresses allows for significant transformation to occur in the previously protective oxide close to the interface. This could lead to the formation of cracks and pores, which can connect with the outer porous layer and the lateral cracks, providing a fast track for diffusing species and causing a transition in the corrosion kinetics.

5. Conclusions

Despite the relatively small area of investigation, the results presented in this work give a significant insight into the mechanisms of the formation of zirconium oxide on Zircaloy-4 in PWR-like conditions. State-of-the-art grain mapping techniques have reliably revealed the morphology, phase and orientation of oxide grains formed on a Zircaloy-4 sample during aqueous corrosion. This work will now allow for the comparison of oxide microstructure and grain boundary characteristics on a variety of different alloys in an attempt to understand how the transformation from tetragonal to monoclinic oxide affects corrosion kinetics. It is also hoped that comparisons can be made between alloys that exhibit different hydrogen pickup behaviour in an attempt to identify the route of hydrogen pickup through the protective oxide layer. The main conclusions are as follows:

- Both measurement techniques have provided consistent results regarding grain orientation of the monoclinic phase. While t-EBSD allowed for misorientation distribution analysis, the TEM method with its superior spatial resolution enables grain boundary characterisation in the oxide and reliable characterisation of the equiaxed tetragonal grains as small as ~5 nm.
- The majority of the oxide grain boundary network formed on Zircaloy-4 consists of 90° and 180° transformation twins, with 90.8° and 180° rotations about the [0 0 1] direction being the most common identified twin boundary in monoclinic zirconium oxide. The high fraction of twin boundaries throughout the oxide demonstrates that the tetragonal-to-monoclinic transformation is a continuous local process. Also, long twin boundaries indicate that some tetragonal grains are allowed to grow significantly above the critical size for stabilization before transformation occurs.
- The observed fibre texture of the monoclinic phase with the $(10\bar{3})$ parallel to the metal–oxide interface occurs due to transformation from tetragonal grains and seems to be a result of the preferred growth of suitably oriented tetragonal grains and the crystallographic relationship between the tetragonal and monoclinic phase.
- In the early stages of oxidation, the transformation is not detrimental to corrosion performance. As the growth front slows and lateral cracks develop, a critical stress level is reached, causing significant transformation and deterioration in the previously protective oxide close to the metal–oxide interface.

Acknowledgments

Funding for this work by AMEC and Rolls Royce plc is gratefully acknowledged. We are grateful to Mr William Smith for assistance in the FIB preparation of the sample used in this work. This research was supported by the Engineering and Physical Sciences Research Council UK (EPSRC) through the Centre for Doctoral Training in Advanced Metallic Systems. The project is part of the MUZIC-2 collaboration studying hydrogen pickup mechanisms in Zr alloys. We also wish to acknowledge the infrastructural support of the University of Manchester's Materials Performance Centre.

References

[1] Yilmazbayhan A, Breval E, Motta AT, Comstock RJ. J Nucl Mater 2006;349:265.
[2] Godlewski J, Gros J, Lambertin M, Wadier J, Weidinger H. In: Zircon. Nucl. Ind. Ninth Int. Symp. ASTM STP 1132; 1991.
[3] Glavicic M. Development and application of techniques for the microstructural characterisation of hydrogen permeability in zirconium oxides. Montreal: McGill University; 1998.
[4] Efsing P, Pettersson K. In: Zircon. Nucl. Ind. Twelfth Int. Symp. ASTM STP 1354; 2000.
[5] Trimby PW. Ultramicroscopy 2012;120:16.
[6] Suzuki S. JOM 2013;65:1254.
[7] Zaefferer S. Cryst Res Technol 2011;46:607.
[8] Lin J, Li H, Szpunar JA. Mater Sci Eng A 2004;381:104.
[9] Petigny N, Barberis P, Lemaignan C, Ch V, Lallemant M. J Nucl Mater 2000;280:318.
[10] Garner A, Preuss M, Frankel P. J Appl Crystallogr 2014;47:575.
[11] Lin J. Effect of texture and microstructure of zirconium alloys on their oxidation and oxide texture. Montreal: McGill University; 2005.
[12] Li H, Glavicic M, Szpunar JA. Mater Sci Eng A 2004;366:164.
[13] Gong W, Zhang H, Qiao Y, Tian H, Ni X, Li Z, et al. Corros Sci 2013;74:323.
[14] Kim HG, Park JY, Choi BK, Jeong YH. J Nucl Mater 2008;374:204.
[15] Gertsman VY, Lin YP, Zhilyaev AP, Szpunar JA. Philos Mag A 1999;79:1567.
[16] Ni N, Hudson D, Wei J, Wang P, Lozano-Perez S, Smith GDW, et al. Acta Mater 2012;60:7132.
[17] Preuss M, Frankel P, Lozano-Perez S, Hudson D, Polatidis E, Ni N, Wei J. Zircon Nucl Ind – 16th Int Symp ASTM STP1529, vol. 8; 2011. p. 1.
[18] Blat-Yrieix M, Ambard A, Foct F, Miquet A, Beguin S, Cayet N. J ASTM Int 2009;5:594.
[19] Platt P, Frankel P, Preuss M, Gass M, Bamber M, Symington I, Howells R. In: Proc. Top Fuel. Manchester; 2012.
[20] Polatidis E, Frankel P, Wei J, Klaus M, Comstock RJ, Ambard A, et al. J Nucl Mater 2013;432:102.
[21] Heuer AH, Ruhle M. Acta Metall 1985;33:2101.
[22] Rudling P, Wikmark G. J Nucl Mater 1999;265:44.
[23] Jin X-J. Curr Opin Solid State Mater Sci 2005;9:313.
[24] Platt P, Frankel P, Preuss M, Gass M, Howells R. *J Nucl Mater* 2014, accepted for publication.
[25] Bailey J, Proc R, Soc A. Math Phys Eng Sci 1964;279:395.
[26] Cox B. J Nucl Mater 2005;336:331.
[27] Garzarolli F, Seidel H, Tricot R, Gros J. In: Zircon. Nucl. Ind. Ninth Int. Symp. ASTM STP 1132; 1991.

[28] Mayer J, Giannuzzi LA, Kamino T, Michael J. MRS Bull 2007;32:400.
[29] Yilmazbayhan A. J Nucl Mater 2004;324:6.
[30] Rauch EF, Dupuy L. Arch Metall Mater 2005;50:87.
[31] Rauch E, Véron M. Microsc Anal 2008;22:S5.
[32] Hull AW. Phys Rev 1921;18:88.
[33] McCullough JD, Trueblood KN. Acta Crystallogr 1959;12:507.
[34] Bondars B, Heidemane G, Grabis J. J Mater sci 1995;30:1621.
[35] Motta AT, Yilmazbayhan A, Comstock RJ, Partezana J, Sabol GP, Lai B, Cai Z. In: Zircon. Nucl. Ind. Fourteenth Int. Symp. ASTM STP 1467, vol. 2; 2005.
[36] Kocks UF, Tome CN, Wenk HR. Texture and anisotropy: preferred orientations in polycrystals and their effect on materials properties. Cambridge: Cambridge University Press; 1998.
[37] Kelly PM, Rose LRF. Prog Mater Sci 2002;47:463.
[38] Barberis P. J Nucl Mater 1995;226:34.
[39] Szpunar JA, Qin W, Li H, Kiran Kumar NAP. J Nucl Mater 2012;427:343.
[40] Gertsman VY, Zhilyaev AP, Szpunar JA. Scr Mater 1996;35:1247.
[41] Wei J, Frankel P, Polatidis E, Blat M, Ambard A, Comstock RJ, et al. Acta Mater 2013;61:4200.
[42] Garvie RC. J Phys Chem 1978;82:218.
[43] Kelly PM, Ball CJ. J Am Ceram Soc 1986;69:259.
[44] Subbarao EC. Phys Status Solidi 1974;9:9.
[45] Ploc RA. J Nucl Mater 1983;13:75.
[46] Motta AT. JOM 2011;63:59.
[47] Guillen R, Cossu C, Franc M, Girard E. J Nucl Mater 1998;255:174.
[48] Mamivand M, Zaeem MA, El Kadiri H, Chen L-Q. Acta Mater 2013;61:5223.
[49] Ni N, Lozano-Perez S, Jenkins M, English C, Smith GD, Sykes J, et al. Scr Mater 2010;62:564.
[50] Gertsman VY, Zhilyaev AP, Szpunar JA. Model Simul Mater Sci Eng 1997;5:35.
[51] Bossis P, Lefebvre F, Barberis P, Galerie A. Mater Sci Forum 2001;369–372:255.